Available online at www.sciencedirect.com
SCIENCE DIRECT®
Lithos 71 (2003) 81–98
LITHOS
www.elsevier.com/locate/lithos

Accessory titanite: an important carrier of zirconium in lamprophyres

Wolfgang Seifert*, Wolfgang Kramer

GeoForschungsZentrum Potsdam, D-14473 Potsdam, C 123, Telegrafenberg, Germany

Received 4 March 2003; accepted 21 July 2003

Abstract

The chemical composition of minerals from a suite of Variscan lamprophyres (kersantite, minette, spessartite and vogesite) from the Saxothuringian Zone of the Variscan orogen, Germany, were investigated by electron microprobe. These lamprophyres usually contain small grains (< 50 μm) of Zr-bearing titanite as the only primary mineral containing traceable zirconium. A late-stage residual alkaline melt within the lamprophyric magma is considered to have crystallized the Zr-rich titanite. The titanite typically has euhedral Zr-rich cores, mantled by Zr-poor overgrowths. This compositional change is explained by rapid decrease of temperature during magma uprise and emplacement. Relatively high Zr contents and compositional and textural heterogeneities (e.g. syenitic schlieren, veins and globules) within the lamprophyric host rocks are evidence of magma mixing.

Incorporation of Zr into titanite apparently takes place as a coupled substitution ($Ti^{4+} + Al^{3+} \Leftrightarrow Zr^{4+} + Fe^{3+}$) rather than as a simple 1:1 replacement of Ti by Zr. A ZrO_2 content of about 6 wt.% (equivalent to ~ 0.10 atoms per formula unit Zr) is implied as the upper concentration limit in titanite. Locally occurring higher values are attributed to tiny inclusions of secondary Zr phases. In carbonate-rich portions of lamprophyres, titanite is transformed into an unindentified TiO_2 phase. High-(Al,F) titanite (X_{Al} up to 0.54), restricted in occurrence to the contact between tonalite porphyry and kersantite, formed under the conditions of high fluorine activity connected with the rhyolitic magmatism.

The results show that the Zr budget of lamprophyres, and possibly of other mafic igneous rocks lacking zircon, is strongly governed by titanite. Element distribution patterns in titanite are a key to the better understanding of magmatic evolution and petrogenesis of lamprophyres.

Keywords: Titanite; Zirconium; Mineral zoning; Lamprophyre; Magma mixing

1. Introduction

Titanite constitutes a widespread accessory mineral in igneous and metamorphic rocks. Due to its capability for element substitutions, titanite acts as an important carrier of trace elements in many rocks. Experimentally determined titanite/liquid partition coefficients for trace elements in a lamproitic system (Tiepolo et al., 2002) show a high susceptibility for the rare earth (RE) and high-field-strength (HFS) elements to become fixed in titanite. Titanite is considered as a potential petrogenetic indicator and, owing to uranium and thorium incorporation, it may be a useful geochronometer (Frost et al., 2000, and references therein).

* Corresponding author. Tel.: +49-331-2881375; fax: +49-331-2881370.
E-mail address: ws@gfz-potsdam.de (W. Seifert).

0024-4937/$ - see front matter © 2003 Elsevier B.V. All rights reserved.
doi:10.1016/j.lithos.2003.07.002

Based on previous studies of lamprophyres (Kramer and Seifert, 1994, 1995), we undertook a systematic search for titanite, which has been observed in 13 of 14 investigated samples. Zr-rich titanite occurs as small-sized grains (10–50 μm) within the groundmass and is hard to recognize optically. That may be the reason why titanite hitherto was overlooked in such rocks. Although Zr concentrations in the studied lamprophyres are fairly high (223–675 ppm), primary formed zircon has never been identified. Compared to other Zr-rich titanites, almost exclusively found in foid-bearing alkaline rocks (Smith, 1970; Giannetti and Luhr, 1983; Flohr and Ross, 1990; Woolley et al., 1992; Dawson et al., 1994; Della Ventura et al., 1999), titanite of the lamprophyres studied here attain the highest Zr concentrations (~ 6 wt.% ZrO_2). The same order of magnitude for Zr in titanite (max. 7.6 wt.% ZrO_2) was reported by Chakhmourdian and Zaitsev (2002) from the ultramafic–alkaline–carbonatitic Afrikanda complex, Kola Peninsula.

The purpose of the present study is (1) to provide the first data on the compositional variability of titanite from lamprophyres, sampled from the Saxo-thuringian Zone of the Mid-European Variscides, and (2) to find controlling factors favouring Zr incorporation into lamprophyric titanite.

2. Sample descriptions

2.1. Geological setting and sampling sites

A schematic geological sketch map and the sampling localities are given in Fig. 1. Detailed sample descriptions are given in Appendix A. The greater part of the *lamprophyre* samples comes from the Henneberg granite quarry near Lehesten (Franken-

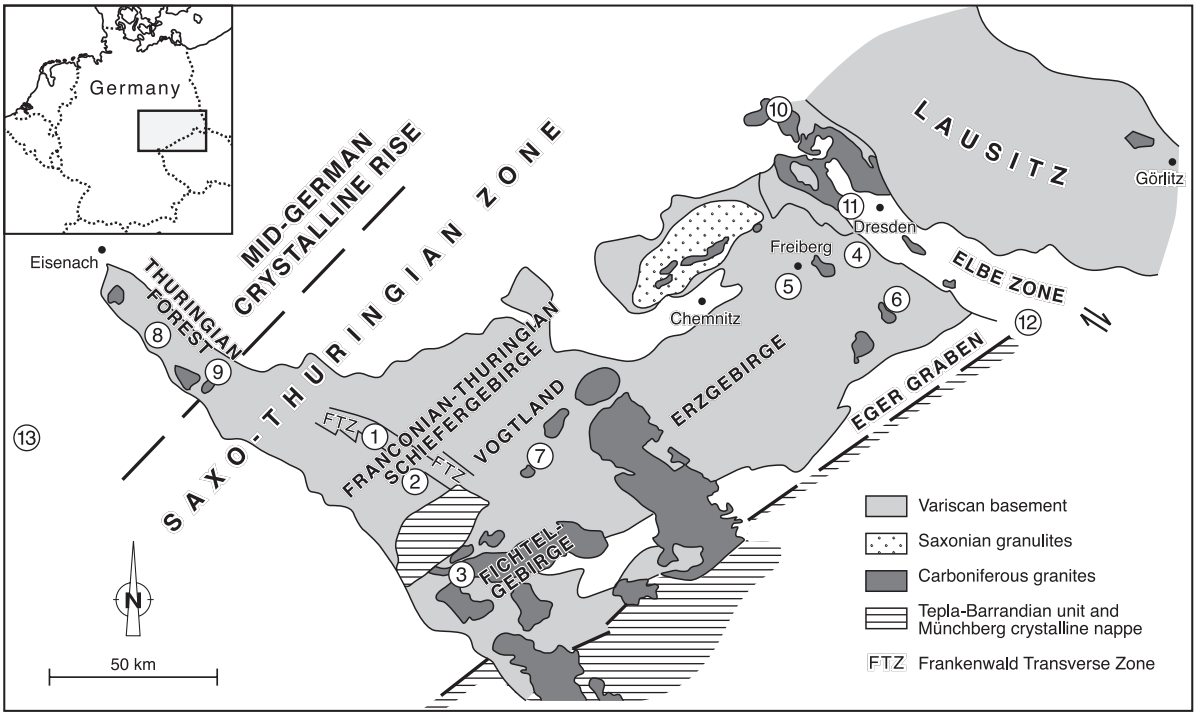

Fig. 1. Sketch map of geological units and sample localities. (1) Henneberg and Bärenstein near Lehesten, (2) Eisenbach valley near Schwarzenbach am Wald, (3) Weissenstadt, (4) Rabenauer Grund, (5) Brand-Erbisdorf, (6) Bärenstein near Altenberg, (7) Tirschendorf, (8) Elmenthal near Trusetal and Höhnberg near Schnellbach, (9) Schmiedefeld, (10) Gröba, (11) Freital, (12) České středohoří Mts., (13) Schackau/Rhön.

wald Transverse Zone) in the Franconian-Thuringian Schiefergebirge. This quarry exposes a small granitic to granodioritic intrusion crosscut by *tonalite porphyry* (*rhyolite*) and numerous lamprophyre dykes comprising the whole compositional diversity of the lamprophyres sensu stricto (Wimmenauer, 1973): *kersantite, minette, spessartite and vogesite*. Vogesite occurs as syenitic schlieren within a kersantite. The term "vogesite" is used because of high portions of pargasite and K-feldspar within the schlieren. The NW–SE striking lamprophyric dykes cut the post-kinematic Henneberg granite (consolidated at 296 ± 3 Ma, Rb/Sr mineral data of Glodny, 1997) but not the neighbouring Zechstein sediments. Further sample localities of lamprophyres are Bärenstein, close to Henneberg, the Eisenbach valley near Schwarzenbach am Wald (Frankenwald), Weissenstadt (Fichtelgebirge) and three occurrences of the Eastern Erzge-

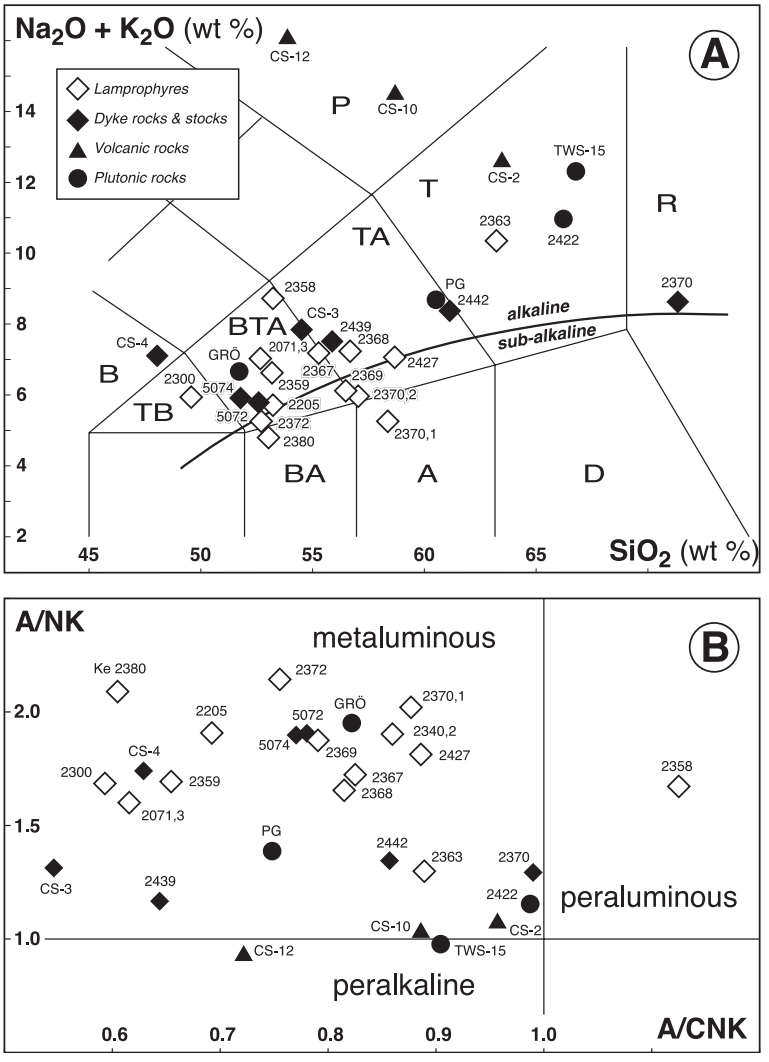

Fig. 2. Characterization of the whole-rock chemistry. (A) TAS diagram after Le Maitre et al. (1989), with alkalic/sub-alkalic line according to Miyashiro (1978). Letters stand for: (B) basanite, (P) phonolite, (TB) trachybasalt, (BTA) basaltic trachyandesite, (TA) trachyandesite, (T) trachyte, (BA) basaltic andesite, (A) andesite, (D) dacite, (R) rhyolite. (B) Alumina-alkali saturation diagram. A/NK = Al/(Na + K) and A/CNK = Al/(Ca + Na + K) in molar proportions.

birge (Rabenauer Grund near Freital, Brand-Erbisdorf near Freiberg, and Bärenstein near Altenberg).

Other igneous rocks (see Appendix A) were selected from several aspects for the comparison of the titanite chemistry. Thus, rocks of different alkalinity, crystallization level (dyke rock, volcanitic, plutonic) and tectonic environment are considered. With the exception of the tonalite porphyry 2370, no other rocks are spatially related to the lamprophyres. The syenite TWS-15 is a basement xenolith sampled from a Tertiary basalt in the Rhön. The alkaline lamprophyre camptonite and the alkaline volcanitic rocks are rift-related Cenozoic rocks from the crossing area of the Eger graben and the Elbe Zone (Northern Bohemia, Czech Republic). Microsyenodiorite, microsyenite and monzodiorite were included in the comparative study because of closest rock–chemical relationship to the lamprophyres.

2.2. Mineral assemblages and textures

Trioctahedral mica is the main mafic phase in minette and kersantite lamprophyres. It is present in two generations: (1) of phlogopite phenocrysts showing zoning with reversals in the Mg/Fe ratio, and (2) of Mg-rich annite flakes in the groundmass. The phenocrysts often display an increase in Ti and Fe from the core to the rim. Some mica phenocrysts show rutile exsolutions forming "sagenite" textures. Spessartite and vogesite lamprophyres typically have amphibole phenocrysts of pargasitic to magnesio-hastingsitic composition. Clinopyroxene occurs as diopside and augite in the lamprophyres. Besides magnetite and titanomagnetite, apatite is the most important accessory mineral in these rocks. Chromian spinel occasionally crystallized in kersantite. All but one of the lamprophyres investigated contain titanite as small crystals in a fine-grained groundmass mainly composed of plagioclase, alkali feldspar, chlorite, titanomagnetite and mafic minerals like phenocrysts. It is assumed that the titanite formed late in the crystallization history because it has not been observed as inclusions in early-formed phenocrysts. The grain diameter of titanite rarely exceeds 50 μm. Titanite mainly has core-rim zonation visible in back-scattered electron (BSE) images (see Section 5.2.2). The different brightness in the BSE images corresponds to variation in composition.

In some places, lamprophyres show schlieren and globular textures indicating distinct heterogeneities due to magma mixing and liquid immiscibility. K-feldspar predominates within syenitic veinlets,

Table 1
Major element and Zr concentrations of representative rock samples

Rock type	Lamprophyres				Dyke rocks and stocks			Plutonic rocks	
Sample	kersantite	minette	spessartite	vogesite	tonalite porph.	microsyenod.	microsyenite	syenite	syenite
Comment	2370.1	2359	2369	2363	2370	5072	2439 in dolerite	2422	TWS-15 xenolith
SiO_2 (wt.%)	54.50	49.10	53.00	60.70	69.10	50.00	54.63	65.15	65.30
TiO_2	1.10	1.34	1.19	0.60	0.24	2.70	2.10	0.48	0.24
Al_2O_3	14.60	13.20	14.70	16.00	14.20	14.20	12.44	16.39	16.85
Fe_2O_3	7.13	7.93	6.92	3.99	1.71	2.70	9.21	1.80	1.32
FeO						8.40	4.46	1.15	0.61
MnO	0.14	0.14	0.13	0.12	0.05	0.14	0.21	0.12	0.34
MgO	5.10	6.78	5.37	1.79	1.05	4.40	1.94	0.98	0.21
CaO	5.19	6.84	5.94	3.20	1.85	5.90	4.78	1.37	0.78
Na_2O	3.26	1.92	2.62	2.55	3.56	2.60	4.70	4.24	7.34
K_2O	1.68	4.20	3.20	7.37	4.75	2.90	2.65	6.57	4.76
P_2O_5	0.84	1.01	0.90	0.23	0.43	1.22	0.74	0.15	0.06
CO_2	0.81	3.86	1.26	0.64	0.27	1.40	0.17	0.05	0.65
H_2O	3.31	3.25	2.77	1.07	1.23	3.20	1.49	0.98	0.59
Total	97.66	99.57	98.00	98.26	98.44	99.76	99.52	99.43	99.05
Zr (ppm)	300	308	327	361	82	550	639	638	626

Total iron as Fe_2O_3 if not otherwise indicated.

schlieren and globules. The globules, sometimes rimmed by carbonates, are sitting in a chlorite-rich mafic to ultramafic matrix (Beuge and Kramer, 1977). Carbonate-rich parts of lamprophyres (e.g. globular-textured minettes) carry rutile instead of titanite.

In contrast to the lamprophyres, titanite of the other rocks investigated has a bigger grain size (>100 μm) and is less intensively core-rim zoned. Moreover, several of these rocks lack titanite (see Appendix A), although the rock chemistry is comparable to titanite-bearing rocks.

3. Environment of formation and stability of titanite

Titanite crystallization is controlled by bulk–rock composition and parameters such as *P*, *T* and fluid composition, especially the fugacities of oxygen, CO_2, OH and F. Titanite crystal chemistry often readily responds to changing environmental conditions. In brief, the characteristics of titanite formation and stability in igneous rocks are as follows (Frost et al., 2000): a precondition for titanite crystallization is a sufficiently high Ca/Al ratio of the melt. High Ca activity will stabilize titanite, whereas high Al activity favours the formation of anorthite + ilmenite instead of titanite. Therefore, titanite is most commonly found in metaluminous rocks of intermediate SiO_2 contents (e.g. diorite, granodiorite, syenite), but is rare in peraluminous and peralkaline rocks because of their low Ca/Al ratio. Titanite occurs in relatively oxidized rocks (Wones, 1989) and is formed from H_2O-rich melts rather than H_2O-poor melts. Frost et al. (2000) suggested that titanite from calc-alkaline plutonic rocks crystallized contemporaneously with the hydration of pyroxene to hornblende, either in a late-magmatic stage or during deuteric alteration. The late-magmatic origin of titanite explains why eruptive rocks are poorer in titanite than their plutonic equivalents (Frost and Lindsley, 1991).

Many previous studies have attributed the stability of titanite under high-*P* conditions to the role of Al in the crystal lattice. High-Al titanite ($X_{Al} = Al/(Al + Ti + Fe^{3+}) > 0.25$, according to Oberti et al., 1991) has been reported from eclogites and associated rocks in several metamorphic terranes (e.g. Smith, 1977; Franz and Spear, 1985; Oberti et al., 1991; Carswell et al., 1996; Castelli and Rubatto, 2002). Experimental data (Smith, 1981) showed that increasing pressure and decreasing temperature promote Al incorporation in titanite. However, there are also examples where high-Al titanites crystallized under low-pressure conditions (Enami et al., 1993; Markl and Piazolo, 1999; this work) and vice versa, where low-Al titanite crystallized under ultrahigh-pressure conditions (Ye et al., 2002). Crystal structure and thermodynamic investigations (Troitzsch and Ellis, 1999, 2002) indicate that the titanite structure should be not well suited to incorporate Al and F instead of Ti and O, although experimental results, recently confirmed by Tropper et al. (2002), show complete solid solution of $CaTiOSiO_4$–$CaAlFSiO_4$. In addition, Tropper et al. (2002) concluded that F–Al content of titanite solid solution is controlled by the coexisting mineral assemblage.

4. Substitution mechanisms in titanite

According to the general formula $^{[7]}Ca\ ^{[6]}Ti[O/^{[4]}SiO_4]$, the structure of titanite contains four sites of possible element substitutions (Sahama, 1946; Ribbe, 1982, and references therein):

Ca site: REE, Y, Mn, Fe^{2+}, Sr, Ba, Mg, Na, K, Li, U, Th, Pb;
Ti site: Al, Fe^{3+}, Nb, Ta, Zr, Sn, V, Cr;
Si site: P, Al, 4H;
O1 site: OH, F, Cl.

Iron predominantly occurs in the trivalent state and occupies the Ti site. Substitutions are of different importance and many of the aforementioned elements occur in concentrations below the detection limit of routine electron-microprobe analysis. H and Li are not measurable by electron microprobe. Numerous investigations indicate that the replacement

$$Ti^{4+} + O^{2-} \Leftrightarrow (Al, Fe)^{3+} + (F, OH)^{-} \quad (1)$$

is the substitution mechanism most common in natural titanite. Note, however, that the thermodynamic sta-

Table 2
Representative analyses (wt.%) of titanite

Rock type	Lamprophyres											
	kersantite		kersantite		minette		minette		spessartite		vogesite	
Sample	2370.1	2370.1	2205	2205	2358	2358	2359	2359	2369	2369	2363	2363
Analysis	1	2	3	4	5	6	7	8	9	10	11	12
Comment	c	r	c	r	c	r	c	r	c	r	c	r
P_2O_5	0.03	0.00	0.14	0.04	0.04	0.08	0.01	0.04	0.02	0.03	0.09	0.14
Nb_2O_5	0.37	0.04	0.29	0.97	0.69	0.00	0.66	0.10	0.35	0.02	1.06	1.19
SiO_2	29.25	32.26	29.36	30.02	29.60	31.28	28.35	30.67	29.26	31.05	29.19	29.55
TiO_2	31.43	21.58	31.82	34.74	31.24	29.04	28.41	33.52	33.41	31.12	34.34	33.46
ZrO_2	2.81	0.00	5.89	0.95	2.06	0.00	9.80	0.00	2.14	0.00	2.27	0.17
Al_2O_3	1.59	12.70	1.19	1.44	2.46	7.44	0.94	3.90	1.55	5.62	0.91	2.10
Fe_2O_3	3.32	0.69	1.91	1.77	3.42	0.78	2.73	1.36	3.39	1.51	2.23	2.48
Y_2O_3	0.25	0.01	0.00	0.02	0.12	0.01	0.25	0.01	0.20	0.04	0.35	0.17
La_2O_3	0.30	0.05	0.49	0.00	0.40	0.10	0.25	0.00	0.47	0.00	0.28	0.50
Ce_2O_3	1.44	0.20	1.01	0.21	0.92	0.15	1.00	0.08	1.15	0.00	1.43	1.47
CaO	25.54	29.18	26.18	27.31	25.93	28.33	22.94	27.70	25.98	28.23	26.12	26.31
MnO	0.10	0.01	0.03	0.00	0.14	0.09	0.02	0.06	0.08	0.04	0.07	0.27
Na_2O	0.03	0.01	0.01	0.03	0.04	0.04	0.09	0.01	0.03	0.02	0.04	0.01
F	0.31	4.88	0.00	0.10	0.79	2.72	0.28	1.37	0.25	1.83	0.00	0.30
$Total_{corr}$	96.64	99.56	98.32	97.56	97.52	98.91	95.61	98.24	98.17	98.74	98.38	97.99
Formula proportions												
P	0.001	0.000	0.004	0.001	0.001	0.002	0.000	0.001	0.001	0.001	0.003	0.004
Nb	0.006	0.001	0.004	0.015	0.011	0.000	0.011	0.001	0.005	0.000	0.016	0.018
Si	1.007	1.015	1.002	1.006	1.004	1.007	1.021	1.007	0.990	1.006	0.991	0.996
Ti	0.814	0.511	0.817	0.876	0.797	0.703	0.769	0.828	0.850	0.758	0.877	0.848
Zr	0.047	0.000	0.098	0.016	0.034	0.000	0.172	0.000	0.035	0.000	0.038	0.003
Al	0.065	0.471	0.048	0.057	0.098	0.282	0.040	0.151	0.062	0.215	0.036	0.083
Fe^{3+}	0.086	0.016	0.049	0.045	0.087	0.019	0.074	0.034	0.086	0.037	0.057	0.063
Y	0.005	0.000	0.000	0.000	0.002	0.000	0.005	0.000	0.004	0.001	0.006	0.003
La	0.004	0.001	0.006	0.000	0.005	0.001	0.003	0.000	0.006	0.000	0.004	0.006
Ce	0.018	0.002	0.013	0.003	0.011	0.002	0.013	0.001	0.014	0.000	0.018	0.018
Ca	0.942	0.983	0.957	0.981	0.942	0.978	0.885	0.974	0.942	0.980	0.950	0.950
Mn	0.003	0.000	0.001	0.000	0.004	0.002	0.001	0.002	0.002	0.001	0.002	0.008
Na	0.002	0.001	0.001	0.002	0.003	0.002	0.006	0.001	0.002	0.001	0.003	0.001
Sum cations	3.000	3.000	3.000	3.000	3.000	3.000	3.000	3.000	3.000	3.000	3.000	3.000
F	0.034	0.485	0.000	0.011	0.085	0.277	0.032	0.142	0.027	0.187	0.000	0.032
OH	0.117	0.002	0.097	0.091	0.101	0.024	0.082	0.042	0.121	0.064	0.093	0.114
O	4.891	4.527	4.939	4.921	4.861	4.715	4.986	4.839	4.896	4.766	4.946	4.893
Σ F + OH + O	5.042	5.014	5.036	5.023	5.046	5.016	5.100	5.024	5.044	5.017	5.040	5.039
Σ Ca site	0.956	0.985	0.965	0.983	0.956	0.984	0.900	0.977	0.956	0.983	0.965	0.967
Σ Ti site	1.018	0.998	1.016	1.007	1.027	1.005	0.883	1.014	1.039	1.010	1.024	1.015
Σ Si site	1.008	1.015	1.006	1.007	1.005	1.010	1.021	1.008	0.991	1.007	0.994	1.000
X_{Al}	0.067	0.472	0.052	0.058	0.100	0.281	0.045	0.149	0.062	0.213	0.038	0.084
X_F	0.224	0.996	0.000	0.104	0.456	0.919	0.280	0.771	0.181	0.746	0.000	0.219

Analyses of titanite in lamprophyres indicate maximum and minimum ZrO_2 representing core (c) and rim (r) compositions, respectively. Analyses of the tonalite-porphyry titanite indicate minimum and maximum Al_2O_3 corresponding to core and rim, respectively. Routine analytical conditions (15 kV/20 nA) were applied.

Dyke rocks and stocks						Volcanic rocks			Plutonic rocks			Detection limit
tonalite porphyry		microsyenodiorite		microsyenite		trachyte	sodal.phon.	haüy. phon.	monz.dior.	monzonite	syenite	
2370	2370	5072	5074	2439	CS-3	CS-2	CS-10	CS-12	GRÖ	PG	TWS-15	
13	14	15	16	17	18	19	20	21	22	24	25	
c	r											
0.03	0.00	0.01	0.02	0.01	0.10	0.11	0.10	0.07	0.11	0.05	0.19	0.10
1.19	0.22	0.01	0.22	0.09	1.49	0.70	2.10	0.96	0.22	0.34	2.11	0.20
30.63	32.60	31.48	30.90	31.68	28.93	29.03	29.60	30.03	30.35	29.30	28.63	0.03
28.85	18.15	33.96	32.99	30.32	34.01	35.15	33.69	34.59	36.72	36.56	32.02	0.05
0.00	0.00	0.00	0.00	0.52	2.19	0.82	0.91	0.83	0.44	0.00	1.13	0.07
6.80	14.93	3.54	4.36	4.44	1.07	1.26	1.79	1.75	1.26	1.20	1.45	0.04
0.48	0.44	1.96	1.97	1.99	2.13	2.28	1.92	2.22	1.84	2.18	2.96	0.11
0.03	0.00	0.01	0.14	0.21	0.12	0.23	0.18	0.04	0.21	0.09	0.38	0.07
0.00	0.00	0.09	0.02	0.01	0.47	0.49	0.56	0.34	0.11	0.82	0.72	0.23
0.01	0.06	0.14	0.08	0.12	1.39	0.96	1.30	0.61	0.47	2.11	2.64	0.25
28.19	30.10	27.77	27.75	27.06	26.00	26.22	27.08	27.52	27.80	26.29	24.87	0.03
0.03	0.08	0.06	0.04	0.01	0.08	0.22	0.19	0.13	0.13	0.12	0.55	0.10
0.01	0.01	0.00	0.11	0.08	0.16	0.05	0.07	0.04	0.02	0.03	0.15	0.04
2.65	5.16	0.35	0.56	0.92	0.17	0.13	0.00	0.21	0.00	0.01	0.00	0.13
97.78	99.70	99.40	98.92	97.07	98.24	97.60	99.49	99.25	99.68	99.10	97.80	
0.001	0.000	0.000	0.001	0.000	0.003	0.003	0.003	0.002	0.003	0.001	0.006	
0.018	0.003	0.000	0.003	0.001	0.023	0.011	0.032	0.014	0.003	0.005	0.033	
1.004	1.012	1.020	1.002	1.046	0.984	0.984	0.986	0.993	0.995	0.982	0.986	
0.711	0.424	0.828	0.804	0.753	0.870	0.896	0.844	0.860	0.906	0.922	0.829	
0.000	0.000	0.000	0.000	0.008	0.036	0.014	0.015	0.013	0.007	0.000	0.019	
0.263	0.546	0.135	0.167	0.173	0.043	0.050	0.070	0.068	0.049	0.047	0.059	
0.012	0.010	0.048	0.048	0.049	0.055	0.058	0.048	0.055	0.045	0.055	0.077	
0.001	0.000	0.000	0.002	0.004	0.002	0.004	0.003	0.001	0.004	0.002	0.007	
0.000	0.000	0.001	0.000	0.000	0.006	0.006	0.007	0.004	0.001	0.010	0.009	
0.000	0.001	0.002	0.001	0.001	0.017	0.012	0.016	0.007	0.006	0.026	0.033	
0.990	1.001	0.964	0.964	0.958	0.948	0.952	0.966	0.975	0.976	0.944	0.917	
0.001	0.002	0.002	0.001	0.000	0.002	0.006	0.005	0.004	0.004	0.003	0.016	
0.001	0.001	0.000	0.007	0.005	0.011	0.003	0.005	0.003	0.001	0.002	0.010	
3.000	3.000	3.000	3.000	3.000	3.000	3.000	3.000	3.000	3.000	3.000	3.000	
0.275	0.507	0.036	0.057	0.096	0.018	0.014	0.000	0.022	0.000	0.001	0.000	
0.000	0.050	0.147	0.157	0.126	0.079	0.095	0.118	0.101	0.094	0.101	0.135	
4.743	4.441	4.850	4.810	4.810	4.937	4.924	4.907	4.896	4.922	4.932	4.911	
5.017	4.997	5.033	5.025	5.033	5.034	5.032	5.026	5.020	5.016	5.034	5.046	
0.992	1.004	0.967	0.974	0.967	0.969	0.972	0.986	0.986	0.986	0.961	0.959	
1.003	0.983	1.011	1.022	0.985	1.027	1.029	1.009	1.012	1.010	1.029	1.016	
1.005	1.012	1.020	1.002	1.047	0.987	0.987	0.989	0.995	0.998	0.984	0.991	
0.266	0.557	0.134	0.163	0.177	0.044	0.050	0.073	0.069	0.049	0.046	0.061	
1.001	0.910	0.196	0.267	0.432	0.188	0.128	0.000	0.178	0.000	0.010	0.000	

Table 3
Representative analyses (wt.%) of titanite from the minette 2359

Rock type	Minette 2359								Detection limit
Sample Analysis	1	2	3	4	5	6	7	8	
P_2O_5	0.10	0.17	0.04	0.10	0.03	0.04	0.08	0.06	0.09
Nb_2O_5	1.00	1.33	1.55	0.98	0.96	0.59	1.01	0.94	0.06
Ta_2O_5	0.00	0.00	0.00	0.01	0.05	0.00	0.16	0.15	0.07
SiO_2	30.26	29.31	30.18	29.56	29.74	29.61	29.89	28.95	0.03
TiO_2	36.16	30.83	28.67	30.41	29.21	30.50	29.38	28.87	0.03
ZrO_2	1.51	2.22	3.87	4.56	4.97	5.72	6.26	9.49	0.04
HfO_2	0.00	0.00	0.07	0.10	0.17	0.11	0.19	0.28	0.15
ThO_2	0.01	0.06	0.23	0.12	0.06	0.09	0.07	0.04	0.04
UO_2	0.00	0.03	0.01	0.05	0.00	0.00	0.01	0.02	0.04
Al_2O_3	0.96	1.65	1.94	1.11	1.81	1.10	1.37	1.09	0.03
Fe_2O_3	1.38	4.31	4.79	3.80	4.09	3.87	3.38	2.83	0.05
Y_2O_3	0.05	0.36	0.33	0.28	0.25	0.22	0.15	0.11	0.03
La_2O_3	0.02	0.88	0.14	0.93	0.13	0.50	0.19	0.17	0.08
Ce_2O_3	0.26	2.40	0.81	2.44	0.71	1.19	0.76	0.57	0.07
Pr_2O_3	0.02	0.35	0.17	0.29	0.15	0.09	0.08	0.09	0.10
Nd_2O_3	0.36	0.84	0.60	0.91	0.40	0.35	0.35	0.28	0.09
Sm_2O_3	0.08	0.07	0.07	0.11	0.06	0.06	0.06	0.05	0.09
MgO	0.00	0.12	0.20	0.09	0.15	0.10	0.09	0.06	0.03
CaO	27.90	25.48	26.81	25.56	26.82	26.37	26.82	25.78	0.02
MnO	0.06	0.15	0.13	0.14	0.13	0.17	0.14	0.12	0.04
Na_2O	0.00	0.06	0.06	0.05	0.05	0.04	0.08	0.04	0.03
F	0.00	0.17	1.23	0.03	0.64	0.15	0.40	0.00	0.20
Total $_{corr.}$	100.13	100.72	101.38	101.62	100.31	100.81	100.75	99.99	
Formula proportions									
P	0.003	0.005	0.001	0.003	0.001	0.001	0.002	0.002	
Nb	0.015	0.020	0.023	0.015	0.015	0.009	0.015	0.015	
Ta	0.000	0.000	0.000	0.000	0.000	0.000	0.001	0.001	
Si	0.997	0.988	1.002	0.997	0.995	0.994	1.002	0.991	
Ti	0.896	0.782	0.716	0.772	0.735	0.770	0.741	0.743	
Zr	0.024	0.037	0.063	0.075	0.081	0.094	0.102	0.158	
Hf	0.000	0.000	0.001	0.001	0.002	0.001	0.002	0.003	
Th	0.000	0.000	0.002	0.001	0.000	0.001	0.001	0.000	
U	0.000	0.000	0.000	0.000	0.000	0.000	0.000	0.000	
Al	0.037	0.066	0.076	0.044	0.071	0.044	0.054	0.044	
Fe^{3+}	0.034	0.109	0.120	0.096	0.103	0.098	0.085	0.073	
Y	0.001	0.006	0.006	0.005	0.004	0.004	0.003	0.002	
La	0.000	0.011	0.002	0.012	0.002	0.006	0.002	0.002	
Ce	0.003	0.030	0.010	0.030	0.009	0.015	0.009	0.007	
Pr	0.000	0.004	0.002	0.004	0.002	0.001	0.001	0.001	
Nd	0.004	0.010	0.007	0.011	0.005	0.004	0.004	0.003	
Sm	0.001	0.001	0.001	0.001	0.001	0.001	0.001	0.001	
Mg	0.000	0.006	0.010	0.005	0.007	0.005	0.004	0.003	
Ca	0.985	0.921	0.954	0.924	0.961	0.948	0.963	0.946	
Mn	0.002	0.004	0.004	0.004	0.004	0.005	0.004	0.003	
Na	0.000	0.004	0.004	0.003	0.003	0.003	0.005	0.003	
Sum cations	3.000	3.000	3.000	3.000	3.000	3.000	3.000	3.000	
F	0.000	0.018	0.129	0.003	0.068	0.016	0.042	0.000	
OH	0.071	0.157	0.066	0.137	0.107	0.125	0.097	0.117	
O	4.952	4.879	4.832	4.906	4.847	4.889	4.885	4.931	

Table 3 (*continued*)

Rock type	Minette 2359								Detection limit
Sample Analysis	1	2	3	4	5	6	7	8	
Formula proportions									
Σ F+OH+O	5.023	5.054	5.028	5.046	4.998	5.030	5.025	5.048	
Σ Ca site	0.996	0.998	1.000	0.999	0.998	0.992	0.997	0.972	
Σ Ti site	1.007	1.014	0.998	1.003	1.007	1.015	1.001	1.037	
Σ Si site	1.000	0.993	1.003	1.000	0.996	0.995	1.004	0.993	
X_{Al}	0.039	0.069	0.083	0.048	0.078	0.048	0.061	0.051	
X_F	0.000	0.104	0.660	0.023	0.388	0.113	0.304	0.000	

Detailed analytical conditions (20 kV/40 nA) were applied.

bility field of Al-bearing titanite is limited. Actually, Al contents greater than ~14 wt.% Al_2O_3 ($X_{Al}=0.54$) have not yet been described from natural titanite. Other coupled substitutions are as follows:

$$Ca^{2+} + Ti^{4+} \Leftrightarrow Na^{+} + (Nb, Ta)^{5+} \quad (2)$$

(Sahama, 1946);

$$Ca^{2+} + Ti^{4+} \Leftrightarrow REE^{3+} + (Al, Fe)^{3+} \quad (3)$$

(Green and Pearson, 1986);

$$2Ti^{4+} \Leftrightarrow (Nb, Ta)^{5+} + (Al, Fe)^{3+} \quad (4)$$

(Clark, 1974);

$$2Ca^{2+} + Ti^{4+} \Leftrightarrow 2REE^{3+} + Fe^{2+} \quad (5)$$

(Exley, 1980);

$$Al^{3+} + H^{+} \Leftrightarrow Ti^{4+} \text{ and} \quad (6)$$

$$\square + 4H^{+} \Leftrightarrow Si^{4+} \quad (7)$$

(Rosenberg, 1974, experimental results).

For Zr incorporation an isovalent substitution is argued:

$$Ti^{4+} \Leftrightarrow Zr^{4+} \quad (8)$$

(Sahama, 1946; Della Ventura et al., 1999).

5. Results

5.1. Whole-rock chemistry

Rock compositions in part are taken from previous studies and literature (see Appendix A). The chemical variation of the rocks selected for this study is shown in the total alkali versus silica (TAS) diagram (Fig. 2A). Almost all lamprophyres plot in the trachyandesite and basaltic trachyandesite field. The alkalic/subalkalic line illustrates that the greater part of samples represents alkali-rich rocks. Concerning the K content, these are of high-K to shoshonitic character. The A/NK versus A/CNK diagram (Fig. 2B) indicates a metaluminous composition for the majority of samples. Table 1 reports the rock chemistry of representative samples.

5.2. Mineral chemistry of titanite

5.2.1. Analytical methods

Mineral analyses were performed on a CAMECA SX-100 electron microprobe employing the PAP matrix correction program. Analyses were undertaken using different operating conditions: (a) routine analysis with 15 kV acceleration voltage and 20 nA beam current and (b) detailed analysis (20 kV/40 nA). The wavelength-dispersive mode and the 1-μm beam diameter were used in both situations. Counting times on peaks in the routine analysis were 20 s for all elements. Detailed analyses were supplemented by additional nine trace elements. The counting times (in seconds) were Pb (300), U (200), Th (100), REEs, Y, Nb, Ta, Hf, P, (60), Zr, Mn, Fe, Al,

Mg, Na, F (20) and for Ca, Ti, Si (10). Background counts were measured in each case in half the time for peak measurement on both sides of the peak. A total time expense of 30 min results for a detailed analysis, and 4.5 min for a routine analysis. Calibrations were done using standard sets of CAMECA and the Smithsonian Institution (REE phosphates). Detection limits are listed in Tables 2 and 3 (last columns), expressed as wt.% of the oxides, with the exception of fluorine. The formula proportions of titanite were calculated according to the procedure proposed by Franz and Spear (1985). According to that, the normalization of the atomic proportions was performed on the basis of three total cations. All iron was assumed as Fe^{3+} and (OH) was calculated as $(OH)=(Al+Fe^{3+})-F$. Oxygen has been calculated by charge balance considerations as $O=0.5$ [(sum of cation charge) − OH − F].

5.2.2. Compositional variability and mineral zonation

Representative analyses obtained by routine technique and by detailed measurements are shown in Tables 2 and 3, respectively. Variations of Zr in titanite of the whole sample suite are listed in Appendix A. The composition of titanite, especially in lamprophyres, often is highly variable within one sample, corresponding to mineral zonation. Average analyses would not be representative for a sample and, therefore, presentation of analyses with maximum and minimum Zr (Table 2, lamprophyres) is preferred.

Lamprophyric titanite typically has euhedral cores incompletely surrounded by anhedral margins as demonstrated by BSE images (Fig. 3a–d). Both, cores and margins, show complex zonation pattern. Fig. 3e–h represent X-ray element maps of Ti and Zr. The Zr distribution pattern reveals oscillatory zoning (Fig. 3g) and shows that the Zr-richest spots occur at the border between core and Zr-poor marginal zone (Fig. 3h).

The analytical data show that almost all lamprophyres carry titanite with detectable Zr contents. Among the other igneous rocks considered here, only zircon-free alkaline rocks have Zr-bearing titanite (see Appendix A) and, contrary to titanite in lamprophyres, it is lacking in a marked compositional zonation. It seems that zircon and Zr-bearing titanite are mutually exclusive; zircon crystallization apparently scavenges almost all available Zr. This is demonstrated by the behaviour of Zr in the monzodiorite from Gröba, Elbe Zone. Those parts of this rock lacking zircon contain Zr-bearing titanite, whereas parts containing zircon host Zr-poor titanite. Zr distribution to different silicate minerals is restricted to peralkaline rocks as detected in the haüyne phonolite (CS-12), where maximum ZrO_2 contents (wt.%) were detected in melanite (1.34), titanite (0.83) and clinopyroxene (0.13).

Analysis 7 (Table 2) and analysis 8 (Table 3), representing maximum ZrO_2 values approaching 10 wt.%, relate to discrete spots showing most brightness in Zr-mapping images (Fig. 3g and h). These high-Zr spots probably do not represent titanite but a Zr phase. However, the microprobe's spatial resolution is not fine enough for an exact identification of such small (~ 1 μm) areas. The supposition that points with ~ 10 wt.% ZrO_2 do not represent titanite is supported by the ZrO_2 concentration range (0–6%) without any gaps, whereas a gap exists between 6% and 9%. This result is based on a total number of about 100 analyses of Zr-bearing titanite.

Detailed analyses of minette 2359 provide an example for variation of titanite composition within an individual sample. Table 3 shows representative analyses from a total number of 36. Lead contents are generally below the detection limit. Compared to Table 2, due to the more complete analyses (especially REEs), the analytical totals yielded values closer to 100%. The sum of Y_2O_3 and REE_2O_3 (La–Sm) can reach about 5 wt.% (e.g. analysis 4, Table 3). Samarium as well as Ta, Hf and U showed detectable concentrations only in a few analyses. A slight excess of cations in the Ti-site, on the one hand, and a slight deficit in the Ca-site, on the other hand, possibly indicate that small amounts of Fe^{2+} are also present.

Niobium and Ce vary from below the detection limit up to the percentage level, whereas phosphorus and sodium mostly remain below the detection limit in the lamprophyric titanite. A high MnO content (up to 2.6 wt.%) was found for the titanite in the syenite TWS-15, corresponding to high MnO amounts (2–6 wt.%) in associated minerals such as richterite, biotite and titanomagnetite.

A peculiar high-(Al,F) titanite occurs at the sharp contact between tonalite porphyry and kersantite. Distances between analyzed titanites of these different

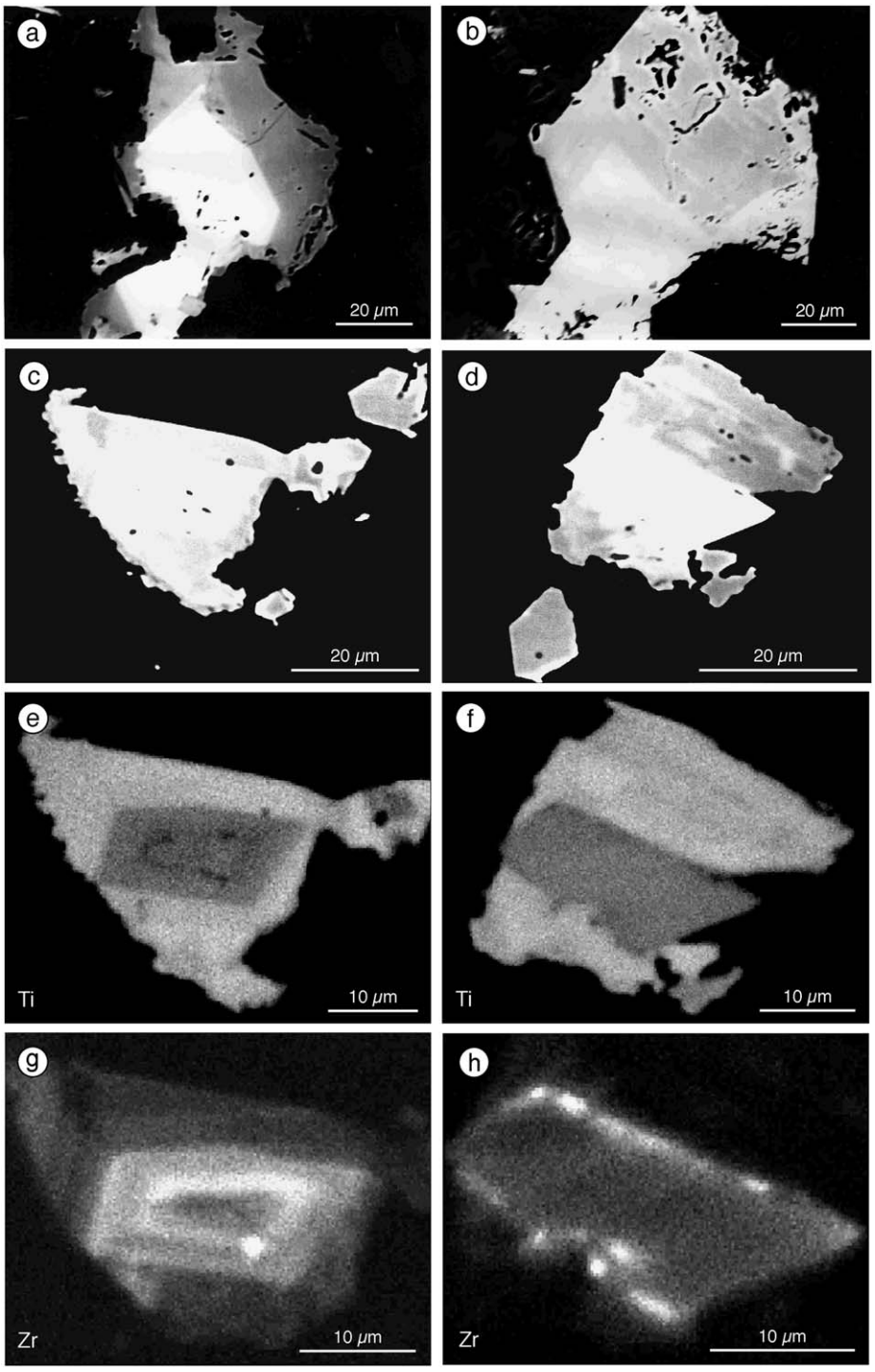

Fig. 3. BSE images (a–d) and element mapping (e–h) of titanite. a) kersantite 2370.1. b) tonalite porphyry 2370. c) and d) minette 2359. e) and f) Ti mapping of the grains in c) and d), respectively. g) and h) Zr mapping of the grains in c) and d), respectively.

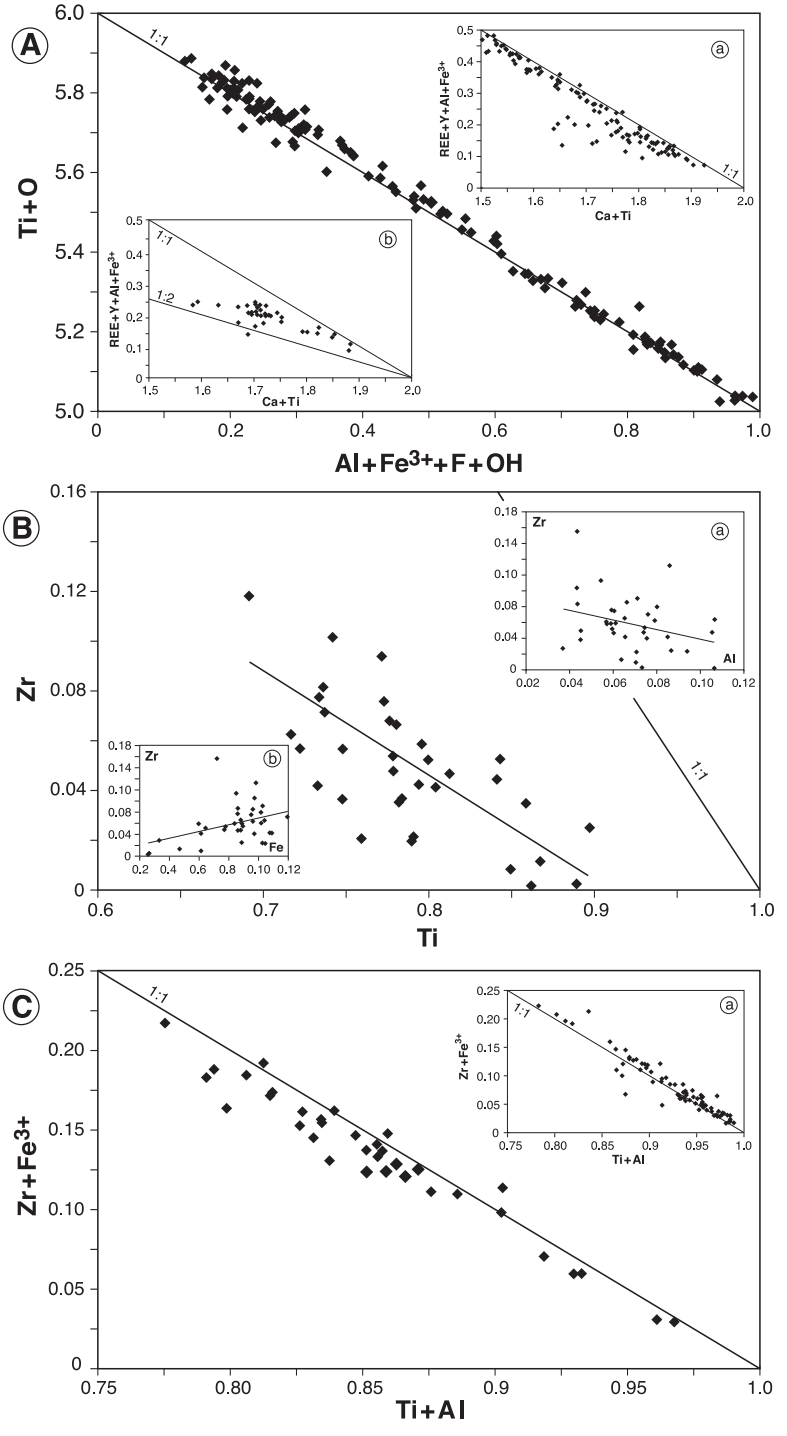
A
Ti+O
Al+Fe3+ +F+OH
1:1
REE+Y+Al+Fe3+
Ca+Ti
a
b
1:2
B
Zr
Ti
Al
Fe
C
Zr+Fe3+
Ti+Al

rocks are no longer than specimen dimension (thin section). Titanite crystals generally are zoned (Fig. 3a and b), showing higher Al amounts in the marginal zones. The average of the five Al-richest titanites (Al_2O_3>13.5 wt.%, marginal analyses), obtained from the tonalitic part of the specimen (sample 2370), yielded $X_{Al}=0.54$, corresponding with the maximum value reported for natural high-Al titanite in the literature. The tonalite porphyry generally has Zr-free titanite, whereas titanite from the kersantitic part of the specimen (sample 2370.1) has Zr-bearing cores and Al-rich rims reaching a maximum of $X_{Al}=0.47$ (Table 2, analysis 2). The F content of the Al-richest titanites varies between 5 and 6 wt.%.

5.2.3. Element correlations and substitutions

Fig. 4 illustrates correlations of elements in the studied titanite. A strong negative correlation ($R=-0.9952$) between (Ti + O) and ($Al+Fe^{3+}+F+OH$), shown in Fig. 4A, indicates that scheme (1) (see Chapter 4) is the dominant substitution mechanism. A further important substitution occurs according to scheme (3), as follows from the correlation in the insets (a) and (b) in Fig. 4A. Increasing Zr content causes a greater deviation from the 1:1 line. The correlation of Zr with Ti, Al and Fe is shown in Fig. 4B. Although Zr and Ti are negatively correlated, their substitution seems to be more complicated than a simple 1:1 replacement. The indicated trend line is defined by a correlation coefficient of $R=-0.6535$ and is not parallel to the 1:1 line. Insets (a) and (b) in Fig. 4B display a slight negative Zr–Al and slight positive Zr–Fe^{3+} correlation, respectively. Taking into account all these correlations, another probable substitution mechanism is

$$Ti^{4+}+Al^{3+}\Leftrightarrow Zr^{4+}+Fe^{3+} \quad (10)$$

This substitution scheme is demonstrated by Fig. 4C for minette 2359 and for all other lamprophyres (inset a). There is a strict negative correlation ($R=-0.9704$) between (Ti + Al) and ($Zr+Fe^{3+}$), indicating that Zr-rich titanites closely follow a trend defined by the proposed substitution mechanism. Other coupled substitutions than the mechanisms (1), (3), (4), and (10) are not significant in the titanites investigated.

5.2.4. Alteration

Carbonate-rich lamprophyres lack titanite but contain an unidentified TiO_2 phase (rutile or anatase?), which evidently corresponds with the high CO_2 content of the rock. In the case of the kersantite 2380, a substantial portion of the CO_2 (4.4 wt.% CO_2 in the whole rock) possibly comes from the wallrock consisting of Carboniferous limestone. The secondary nature of this TiO_2 phase is confirmed by anhedral grain aggregates of heterogeneous composition. Characteristically, these have considerable SiO_2 values up to 7 wt.% and ZrO_2, Fe_2O_3, Al_2O_3 and CaO contents of about 1 to 2 wt.%, as well as a deficit in the analytical totals. An unusual analysis of an alteration product was obtained from the sample 2380: 43% TiO_2, 24% ZrO_2, 16% SiO_2 including minor amounts of other components as well as an analytical total of 92%. Apparently, this is a mixture of rutile, zircon (baddeleyite?), quartz and carbonate produced by alteration of an earlier formed Zr-rich titanite. Two simplified alteration reactions are suggested depending on whether zircon or baddeleyite is formed:

$$2Ca(Ti_{0.5}Zr_{0.5})[O/SiO_4]+2CO_2 = TiO_2+ZrSiO_4+SiO_2+2CaCO_3 \quad (11)$$

$$2Ca(Ti_{0.5}Zr_{0.5})[O/SiO_4]+2CO_2 = TiO_2+ZrO_2+2SiO_2+2CaCO_3. \quad (12)$$

Fig. 4. Compositional plots of titanite (atoms per formula unit) to test the importance of the substitution mechanisms. (A) Plot of all samples investigated representing the main substitution trend (1) $Ti^{4+}+O^{2-}\Leftrightarrow(Al,Fe)^{3+}+(F,OH)^{-}$, inset (a): substitution schema (3); all samples, routine analyses, inset (b): substitution schema (3); minette 2359, detailed analyses. (B) Correlation of Zr vs. Ti; minette 2359, detailed analyses, inset (a): correlation of Zr vs. Al, inset (b): correlation of Zr vs. Fe^{3+}, (C) Plot of ($Zr^{4+}+Fe^{3+}$) vs. ($Ti^{4+}+Al^{3+}$) representing a complex substitution mechanism typically of Zr-bearing titanites (minette 2359, detailed analyses), inset (a): the same correlation, plot of all lamprophyres.

Unfortunately, there is no information about the temperature conditions for such reactions, which would be of general interest, because low-*T* hydrothermal formation of zircon is unknown till now.

In the minette, 2358 titanite occurs, but in the carbonate-rich (calcitic) globular-textured parts of this sample, only secondary rutile was identified.

6. Discussion

Discontinuous compositional zoning in igneous minerals generally can be attributed to several processes, including inheritance, magma mixing and segregation, changes in PT conditions and crystal/melt element partitioning, discrete events in the crystallization history like incipient crystallization of an additional phase and kinetic effects. All these possible explanations for element zoning in titanite from lamprophyres have to be considered. We focus the discussion primarily on zoning of Zr, Al, Fe^{3+}, F, and Ti, which are responsible for most of the observed compositional variations. Specific zoning features to be considered are: (1) abrupt changes in composition from Zr-rich cores to Zr-poor margins; (2) formation of high-(Al,F) titanite as marginal growth zones around Zr-bearing titanite in kersantite near the contact to the tonalite porphyry. In addition, we have to consider what the source of the relatively high Zr contents in lamprophyres is.

6.1. Inheritance

By analogy to well-known phenomena in zircon, inherited titanite cores, which survived a melting event of a previous host rock, are expected to be rounded or irregularly shaped. However, most titanite cores in the lamprophyres are euhedral. For that reason, Zr-rich cores are not explicable by inheritance from a remelted rock. As another kind of inheritance, we could consider injections of Zr-rich titanite-bearing melts into the lamprophyric melts, where these titanites continued their growth as Zr-poor margins during or after the magma mixing, but there are arguments against this view (see below).

6.2. Magma mixing

Reversals of the Mg/Fe ratio within phlogopite phenocrysts from minettes described by Kramer and Seifert (1994) are interpreted as the result of repeated injections of more primitive melts in deep-seated magma chambers (Mauger, 1988). Several other phenomena, including syenitic schlieren, veinlets and globules (ocelli) in some lamprophyres indicate that syenitic melts played an important role in the petrogenesis of these rocks. Beuge and Kramer (1977) explained these textures by magma mixing between mantle-derived mafic lamprophyres and mid-crustal felsic (syenitic) melts. Due to different properties (e.g. viscosity) of the two melts, a contamination would result in incompletely mixed magma forming syenitic schlieren and globules. Since the Zr concentrations in syenitic parts are higher than in lamprophyric parts, we argue that mid-crustal syenitic melts considerably contributed to the total Zr budget of the lamprophyres. This explains the relatively high Zr contents of the lamprophyres (> 330 ppm on average) compared to < 300 ppm Zr of other mantle-derived rocks (e.g. Tertiary alkali basalts) from the study area. A supply of Zr-rich titanite by syenitic melts into lamprophyres is, however, inconsistent with the observation that syenitic schlieren compared with the host lamprophyres are not distinguished by higher Zr concentrations in titanite. Thus, we have no indications that the core-rim zonation of titanite is due to magma mixing.

6.2.1. Crystal/melt element partitioning and kinetic effects

Paterson and Stephens (1992) gave a detailed report about factors influencing the incorporation of trace elements into a growing crystal such as diffusion rates in the melt, crystal growth rates and crystal/liquid interface kinetics which are responsible for zoning patterns, especially sector zoning, in titanite. Those processes are clearly relevant for trace element partitioning in slowly cooled plutonic rocks of compositions from monzonitic to granitic, but in the case of Zr-rich titanite in lamprophyres, sector zoning was not observed. The weak zoning shown in Fig. 3b and g (oscillatory) and in Fig. 3d (patchy) should be

caused by small-scale fluctuation in rates of crystal growth and diffusion rather than changes in magma chemistry (Shore and Fowler, 1996), but the marked core-rim zonation is probably caused by a rapid decrease of temperature of the uprising magma. After the temperature falling off a continuation of Zr entrance is hindered due to lowered Zr mobility in the melt. Therefore, the Zr-poor overgrowths represent titanite formed in the late- or postmagmatic stage. The general lack of primary zircon in lamprophyres shows that the Zr-saturation concentration (Watson and Harrison, 1983) necessary to form this mineral was never attained in parental lamprophyric melts. This statement may be current until the nature of the Zr-richest spots, occasionally occurring between core and marginal overgrowth of titanite, is clarified. These tiny spots could prove to be zircon or baddeleyite. However, a secondary formation of such Zr phases (e.g. exsolution or alteration) is more probable than a primary crystallization from the melt. The favoured substitution mechanism $Ti^{4+} + Al^{3+} \Leftrightarrow Zr^{4+} + Fe^{3+}$ instead of a simple 1:1 replacement of Ti by Zr in titanite probably is founded on strain compensation (Blundy and Wood, 1994). This may explain why the hypothetical end-member $CaZr[O/SiO_4]$ does not exist in nature.

6.2.2. High-(Al,F) titanite

The occurrence of a high-(Al,F) titanite is restricted to the contact between tonalite porphyry and kersantite in specimen scale. Field observations do not establish the age relation between these rocks. A chilled zone between tonalite and lamprophyre is not evident, which would indicate that both rocks were at or close to thermal equilibrium, and that volatile and fluid exchange may have been possible. This suggests that the formation of high-(Al,F) titanite in kersantite is controlled by an input of fluorine from the (apparently) younger tonalite porphyry. These particular low-*P*, high-*T* titanites formed under the condition of a high-F activity support the conclusions of previous workers (e.g. Carswell et al., 1996; Markl and Piazolo, 1999) that the Al content of titanite is not suitable as a *P*–*T* indicator.

7. Summary

The comparative study of accessory titanite from Variscan lamprophyres and other calc-alkaline and alkaline igneous rocks allows the following conclusions.

(1) In the lamprophyres, titanite generally contains zirconium irrespective of the regional position and chemistry of their host rocks. Occasional lack of titanite is attributed to CO_2-related alteration resulting in Zr-bearing rutile or mixtures of secondary minerals.
(2) Zirconium incorporation into titanite takes place as a coupled isovalent substitution ($Ti^{4+} + Al^{3+} \Leftrightarrow Zr^{4+} + Fe^{3+}$). This replacement extends up to about 6 wt.% ZrO_2 (~0.1 *apfu* Zr) in the lamprophyric titanites studied.
(3) A two-stage growth history of titanite, represented by the abrupt compositional change between Zr-rich cores and Zr-poor marginal growth zones, is attributed to temperature decrease during the magma uprise and emplacement.
(4) A link between the Zr content of the studied lamprophyres and processes of magma mixing is suggested but not proved directly by the present work. No correlation exists between the (maximum) Zr concentration in titanite and that in their host rocks (all rock types).
(5) High-(Al,F) overgrowths of titanite in kersantite close to the contact with tonalite porphyry formed metasomatically under conditions of high fluorine activity connected with the acid (rhyolitic) magmatism.

Acknowledgements

We thank Hans-Jürgen Förster (Univ. Potsdam) and Johannes Glodny (GFZ Potsdam) for helpful suggestions for the manuscript and improvement of the grammar. Technical advice by Dieter Rhede (GFZ) for EMP analysis and imaging is gratefully acknowledged. Trevor H. Green (Macquarie Univ. Sydney) and an anonymous reviewer improved the style and content of the final manuscript by constructive comments.

Appendix A. List of samples

Rock types	No. of sample	Geological region/sample location	Reference	Zr in rock (ppm)	Zr in titanite (wt.%)	Notes
Lamprophyres sensu stricto						
Kersantite						
	2368	FTZ/Henneberg	Kramer and Seifert (1995)*	536	0.0–1.0	
	2370.1	FTZ/Henneberg		300	0.0–2.8	
	2370.2	FTZ/Henneberg		317	0.0–3.3	
	2372	FTZ/Henneberg		223	0.0–0.6	
	2380	FW/Schwarzenbach a.W.	Kramer and Seifert (1995)*	675	no titanite	TiO_2
	2205	EE/Rabenauer Grund	Kramer (1976)*	420	0.9–5.9	
Minette						
	2358	FTZ/Henneberg		378	0.0–2.0	TiO_2**
	2359	FTZ/Bärenstein		308	0.0–9.8	
	2071.3	EE/Brand-Erbisdorf	Kramer (1976)*	530	0.0–0.2	
Spessartite						
	2367	FTZ/Henneberg	Kramer and Seifert (1995)*	370	0.0–1.6	
	2369	FTZ/Henneberg		327	0.0–2.3	
	2427	FG/Weissenstadt		238	0.0–0.2	
	2300	EE/Bärenstein	Kramer (1976)*	370	0.0–1.1	
Vogesite						
	2363.1	FTZ/Henneberg	Kramer and Seifert (1995)*	361	0.2–2.3	
Dyke rocks and stocks						
Microsyenodiorite						
	5072	VL/Tirschendorf	Werner (1994)	550	0.0	zircon
	5074	VL/Tirschendorf	Werner (1994)	700	0.0	zircon
Microsyenite						
	2439	TF/Höhnberg	Katzung and Obst (1996)	639	0.0–0.5	
	CS-3	CS/Giegelberg	Ulrych et al. (1998)*	502	0.2–2.2	
Camptonite						
	CS-4	CS/Leština	Ulrych et al. (1998)*	355	no titanite	TiO_2
Syenite porphyry						
	2442	TF/Elmenthal		n.a.	no titanite	zircon
Tonalite porphyry						
	2370	FTZ/Henneberg		82	0.0	
Volcanic rocks						
Trachyte						
	CS-2	CS/Valkeřice	Ulrych et al. (1998)*	540	0.4–0.8	
Sodalite phonolite						
	CS-10	CS/Maršovický vrch Hill	Ulrych et al. (1998)*	726	0.4–1.0	
Haüyne phonolite						
	CS-12	CS/Tachovský vrch Hill	Ulrych et al. (1998)*	891	0.5–0.8	
Plutonic rocks						
Monzodiorite						
	GRÖ	EZ/Gröba	Pfeiffer (1964)*	449	0.0–0.4	zircon
Monzonite						
	PG	EZ/Freital	Pfeiffer (1964)*	384	0.0	zircon
Syenite						
	2422	TF/Schmiedefeld		638	no titanite	zircon
	TWS-15	MGCR/Schackau	Franz and Seifert (1998)	626	0.1–1.3	

Abbreviations for geological regions: CS, Èské stredohoří Mts. (Czech Republic); EE, East Erzgebirge; EZ, Elbe Zone; FG, Fichtelgebirge; FW, Frankenwald; FTZ, Frankenwald Transverse Zone; MGCR, Mid-German Crystalline Rise; TF, Thuringian Forest; VL, Vogtland.*: Whole rock data used in the present work.**: Within globular textured parts.

References

Beuge, P., Kramer, W., 1977. Lamprophyre Ostthüringens und ihre anomalen Quecksilbergehalte im Ergebnis endogener und exogener Anreicherungsprozesse. Schriftenr. Geol. Wiss., Berlin 8, 79–99.

Blundy, J., Wood, B., 1994. Prediction of crystal-melt partition coefficients from elastic moduli. Nature 372, 452–454.

Carswell, D.A., Wilson, R.N., Zhai, M., 1996. Ultra-high pressure aluminous titanites in carbonate-bearing eclogites at Shuanghe in Dabieshan, central China. Mineral. Mag. 60, 461–471.

Castelli, D., Rubatto, D., 2002. Stability of Al- and F-rich titanite in metacarbonate: petrologic and isotopic constraints from a polymetamorphic eclogitic marble of the Sesia Zone (Western Alps). Contrib. Mineral. Petrol. 142, 627–639.

Chakhmourdian, A.R., Zaitsev, A.N., 2002. Calcite-amphibole-clinopyroxene rock from the Afrikanda complex, Kola Peninsula, Russia: mineralogy and a possible link to carbonatites: III. Silicate minerals. Can. Mineral. 40, 1347–1374.

Clark, A.M., 1974. A tantalum-rich variety of sphene. Mineral. Mag. 39, 605–607.

Della Ventura, G., Bellatreccia, F., Williams, C.T., 1999. Zr- and LREE-rich titanite from Tre Croci, Vico Volcanic complex (Latium Italy). Mineral. Mag. 63, 123–130.

Dawson, J.B., Smith, J.V., Steele, I.M., 1994. Trace-element distribution between coexisting perovskite, apatite and titanite from Oldoinyo Lengai, Tanzania. Chem. Geol. 117, 285–290.

Enami, M., Suzuki, K., Liou, J.G., Bird, D.K., 1993. Al–Fe^{3+} and F–OH substitutions in titanite and constraints on their P–T dependence. Eur. J. Mineral. 5, 219–231.

Exley, R.A., 1980. Microprobe studies of REE-rich accessory minerals: implications for Skye granite petrogenesis and REE mobility in hydrothermal systems. Earth Planet. Sci. Lett. 48, 97–110.

Flohr, J.K., Ross, M., 1990. Alkaline igneous rocks of Magnet Cove, Arkansas: mineralogy and geochemistry of syenites. Lithos 26, 67–98.

Franz, L., Seifert, W., 1998. Basement studies in a continental suture zone—xenoliths from the Mid-German Crystalline Rise (Rhön area Mid-European Variscides). N. Jb. Miner. Abh. 173, 263–303.

Franz, G., Spear, F.S., 1985. Aluminous titanite (sphene) from the eclogite zone, south-central Tauern window. Austria Chem. Geol. 50, 33–46.

Frost, B.R., Lindsley, D.H., 1991. Occurrence of iron–titanium oxide minerals in igneous rocks. Rev. Mineral. 25, 433–486.

Frost, B.R., Chamberlain, K.R., Schumacher, J.C., 2000. Sphene (titanite): phase relations and role as a geochronometer. Chem. Geol. 172, 131–148.

Giannetti, B., Luhr, J.F., 1983. The white trachytic tuff of Roccamonfina Volcano (Roman Region Italy). Contrib. Mineral. Petrol. 84, 235–252.

Glodny, J., 1997. Der Einfluß von Deformation und fluidinduzierter Diaphthorese auf radioaktive Zerfallssysteme in Kristallingesteinen. Dissertation, Univ. Münster.

Green, T.H., Pearson, N.J., 1986. Rare-earth element partitioning between sphene and coexisting silicate liquid at high pressure and temperature. Chem. Geol. 55, 105–119.

Katzung, G., Obst, K., 1996. Spätvariszischer basischer Magmatismus-der Höhenberg-Sill im Thüringer Wald. Z. Dtsch. Geol. Ges. 147, 11–38.

Kramer, W., 1976. Genese der Lamprophyre im Bereich der Fichtelgebirgisch- Erzgebirgischen Antiklinalzone. Ein geochemisch-petrologischer Beitrag zum Problem der Kruste-Mantel-Beziehungen. Chem. Erde 35, 1–49.

Kramer, W., Seifert, W., 1994. Mica-lamprophyres and related volcanics of the Erzgebirge and metallogenetic aspects. In: Seltmann, R., Kämpf, H., Möller, P. (Eds.), Metallogeny of Collisional Orogens. Czech Geological Survey, Prague, pp. 159–165.

Kramer, W., Seifert, W., 1995. New data on lamprophyres from Gümbel's type locality. Zbl. Geol. Paläont. Teil I H.5/6, 503–507.

Le Maitre, R.W. (Ed.), 1989. A classification of igneous rocks and glossary of terms. Recommendations of the International Union of Geological Sciences Subcommission on the Systematics of Igneous Rocks. Blackwells, Oxford. 193 pp.

Markl, G., Piazolo, S., 1999. Stability of high-Al titanite from low-pressure calcsilicates in light of fluid and host-rock composition. Am. Mineral. 84, 37–47.

Mauger, R.L., 1988. Ocelli: transient disequilibrium features in a lower carboniferous minette near Concord, North Carolina. Can. Mineral. 26, 117–131.

Miyashiro, A., 1978. Nature of alkalic volcanic rock series. Contrib. Mineral. Petrol. 66, 91–104.

Oberti, R., Smith, D.S., Rossi, G., Caucia, F., 1991. The crystal-chemistry of high-aluminium titanites. Eur. J. Mineral. 3, 777–792.

Paterson, B.A., Stephens, W.E., 1992. Kinetically induced compositional zoning in titanite: implications for accessory-phase/melt partitioning of trace elements. Contrib. Mineral. Petrol. 109, 373–385.

Pfeiffer, L., 1964. Beiträge zur Petrologie des Meißner Massivs. Freib. Forsch.hefte, C 179, 1–222.

Ribbe, P.H., 1982. Titanite. In: Ribbe, P.H. (Ed.), Orthosilicates. Mineral. Soc. Am. Rev. Mineral., vol. 5, pp. 137–154.

Rosenberg, P.E., 1974. Compositional variations in synthetic sphene. Geol. Soc. Am. Abstr. Prog. 6, 1060.

Sahama, Th.G., 1946. On the chemistry of the mineral titanite. Bull. Comm. Geol. Finl. 138, 88–120.

Shore, M., Fowler, A.D., 1996. Oscillatory zoning in minerals: a common phenomenon. Can. Mineral. 34, 1111–1126.

Smith, A.L., 1970. Sphene, perovskite and coexisting Fe–Ti oxide minerals. Am. Mineral. 55, 264–269.

Smith, D.C., 1977. Aluminium bearing sphene in eclogites from Sunnmøre (Norway). Geolognytt 10, 32–33.

Smith, D.C., 1981. The pressure and temperature dependence of Al-solubility in sphene in the system Ti–Al–Ca–Si–O–H. Prog. Exp. Petrol. 18, 193–197.

Tiepolo, M., Oberti, R., Vannucci, R., 2002. Trace-element incorporation in titanite: constraints from experimentally determined solid/liquid partition coefficients. Chem. Geol. 191, 105–119.

Troitzsch, U., Ellis, D.J., 1999. The synthesis and crystal structure

of $CaAlFSiO_4$, the Al–F analog of titanite. Am. Mineral. 84, 1162–1169.

Troitzsch, U., Ellis, D.J., 2002. Thermodynamic properties and stability of AlF-bearing titanite $CaTiOSiO_4$–$CaAlFSiO_4$. Contrib. Mineral. Petrol. 142, 543–563.

Tropper, P., Manning, C.E., Essene, E.J., 2002. The substitution of Al and F in titanite at high pressure and temperature: experimental constraints on phase relations and solid solution properties. J. Petrol. 43, 1787–1814.

Ulrych, J., Cajaz, V., Adamovič, J., 1998. Magmatism and rift basin evolution. Excursion guide. Czech Geol. Surv., Prague. 59 pp.

Watson, E.B., Harrison, T.M., 1983. Zircon saturation revisited: temperature and composition effects in a variety of crustal magma types. Earth Planet. Sci. Lett. 64, 295–304.

Werner, C.-D., 1994. A Permosilesian intrusion in the southern Vogtland, Saxony. Zbl. Geol. Paläont. Teil I H.5/6, 529–535.

Wimmenauer, W., 1973. Lamprophyre, semilamprophyre und anchibasaltische ganggesteine. Fortschr. Mineral. 51, 3–67.

Wones, D.R., 1989. Significance of the assemblage titanite + magnetite + quartz in granitic rocks. Am. Mineral. 74, 744–749.

Woolley, A.R., Platt, R.G., Eby, N., 1992. Niobian titanite and eudialyte from the Ilomba nepheline syenite complex, north Malawi. Mineral. Mag. 56, 428–430.

Ye, K., Liu, J.-B., Cong, B.-L., Ye, D.-N., Xu, P., Omori, S., Maruyama, S., 2002. Ultrahigh-pressure (UHP) low-Al titanites from carbonate-bearing rocks in Dabieshan-Sulu UHP terrane, eastern China. Am. Mineral. 87, 875–881.